Superconductor Science and Technology

PAPER

Analysis of local burnout in a sub-scale test coil for the 32 T magnet after spontaneous quenches during fast ramping

To cite this article: X Hu *et al* 2022 *Supercond. Sci. Technol.* **35** 075009

IOP Publishing Superconductor Science and Technology
Supercond. Sci. Technol. **35** (2022) 075009 (11pp) https://doi.org/10.1088/1361-6668/ac49a4

Analysis of local burnout in a sub-scale test coil for the 32 T magnet after spontaneous quenches during fast ramping

X Hu[1,*], A A Polyanskii, D V Abraimov, A V Gavrilin, H W Weijers[2], F Kametani, J Jaroszynski and D C Larbalestier

National High Magnetic Field Laboratory, Florida State University, Tallahassee, FL, United States of America

E-mail: xh12@my.fsu.edu

Received 30 September 2021, revised 16 December 2021
Accepted for publication 10 January 2022
Published 25 May 2022

Abstract

Industrial production of $REBa_2Cu_3O_{7-\delta}$ (REBCO) coated conductors has made it possible to construct the 32 T magnet, the first successful all-superconducting user magnet to exceed 30 T, which now serves users as SCM4 (superconducting magnet) at the NHMFL. Here, we present an analysis of the damage that occurred in late-stage proof testing of the 32 T prototype coil after many essential facets of the design had been proven through more than 100 intentionally triggered quenches at fields up to 24 T. This prototype coil was then subjected to accelerated charge–discharge cycles at a rate 44 times faster than its design ramp rate in an attempt to address its fatigue tolerance. The extra hysteresis loss of the fast ramps led to heating of the end pancakes, which was induced after 55 fatigue cycles, three spontaneous quenches at progressively lower currents. Recognizing that the coil was damaged, the pancakes were then unwound and their REBCO tapes run through our continuous in-field transport I_c and remnant-field magnetization monitoring device, YateStar, which revealed three highly localized zones of low I_c in the end pancake that induced quench. Careful examination of these zones, especially the most intensely damaged one, revealed that the worst hot spot reached at least 779 °C during the quenches. Magneto-optical imaging showed that this damaged zone was about 5 mm in diameter and indeed the perpendicular damage length induced in neighboring turns by this localized quench heating was almost as great. Although there is much present concern about fatigue crack propagation from edge defects, we actually attribute this damage not to fatigue but to fluctuations in vortex pinning density due to imperfect $BaZrO_3$ (BZO) nanorod growth that locally reduced the critical current I_c. These localized low-I_c regions then had to shed their excess current into the copper stabilizer, producing intense heating. We provide transmission and scanning electron microscopy evidence for local fluctuations of the BZO pinning structure and relate it to recent work that shows significant variations of 4 K, high field I_c values due to apparent production fluctuations of the growth conditions of the Zr-doped metal-organic chemical vapor deposition REBCO used for this test magnet.

[1] Present address: Southwestern Institute of Physics, Chengdu, China.
[2] Present address: Robinson Research Institute, Victoria University of Wellington, New Zealand.
[*] Author to whom any correspondence should be addressed.

Keywords: coated conductor, insulation coil, spontaneous quench, vortex pinning variations, localized burnout

(Some figures may appear in color only in the online journal)

1. Introduction

The great progress made in the manufacture of $REBa_2Cu_3O_{7-\delta}$ (REBCO, RE = rare earth elements) coated conductors has facilitated the exploration of their applications to ultra-high-field magnets with fields much greater than that is possible with Nb-based conductors [1–9]. Starting from a 26.8 T insert magnet in 2009 [1], records made by REBCO test coils reached 40.2 T in 2016 [10], and 45.5 T in 2017, reported in 2019 [11]. One fact is that the high-field records are closely related to the continued development of the conductors. For example, the self-field I_c (77 K) of 4 mm wide tapes from SuperPower was around 110 A in 2007 [12], 125 A in 2014 [13], and 144 A in 2016 [14]. These tapes use REBCO layer thicknesses of order 1.5–2 μm, but 4 or even 5 μm thick REBCO layers can now be grown with advanced metal-organic chemical vapor deposition (MOCVD) [15], even if such processes are not yet industrialized. The uniformity of the tapes has also improved greatly in recent years [16], although it is not perfect yet. Although cracks or scratches or other types of cross-section reductions used to be thought of as the principal cause of locally degraded J_c, we have found significant evidence for vortex pinning variations being important for I_c variations by performing transport measurements at 77 K with 0.6–1 T field in two orthogonal orientations [16, 17]. As discussed in [18] and [19], the 4 K–30 K properties are determined by the strong correlated pinning generated by $BaZrO_3$ (BZO) and RE_2O_3 at 77 K but the differential strain induced by these pins also produces much matrix disorder that greatly amplifies the J_c at lower temperature. 77 K I_c tests cannot yet directly predict 4 K high field properties but fluctuations in the 77 K vortex pinning properties that are made visible by two-axis I_c measurements do signal when unexpected ratios of 77 K to 4 K properties may be expected.

The 32 T project began in 2009 with the goal to build an all-superconducting, high-field magnet for NHMFL users [20]. In 2012, important design choices like a dry wound, bare conductor with an insulated stainless steel co-wind, and distributed heaters for quench protection, were verified by small test coils [21]. This led to the design of two 32 T REBCO inserts with inner/outer radii of 20/70 mm (coil 1) and 82/116 mm (coil 2) generating 17 T inside a 15 T LTS outsert. The prototype coils discussed here had the same dimensions as the final 32 T design but were axially much shorter [22, 23]. To verify the ability of the custom quench detection and protection system, the prototype coils were deliberately and safely quenched over 100 times by deliberately triggering the heaters (there were no spontaneous quenches during this exercise). After this very successful campaign, it was decided to explore the fatigue behavior, which required much faster-than-design ramp rates in order to get a meaningful number of cycles in reasonable time. During this far-from-normal-service ramping, three spontaneous quenches occurred after 55 cycles, inducing progressive degradation of the quench current [23]. A change in ramp pattern between cycles 55 and 56 preceded the quenches. The coils were then taken out of service and deconstructed so as to better understand what occurred during these last spontaneous and damaging quenches.

1.1. The deconstructed prototype coil after damaging spontaneous quenches

The conductor used for the coils was a standard advanced pinning conductor from SuperPower specially supplied with a thick electro-plated 50 μm (normally it has 20 μm) Cu layer on each side, but the remaining parts of the conductor were standard product (50 μm substrate, 1 to 2 μm Ag on each side and $\sim$1 μm REBCO) that used MOCVD grown Zr-doped $(Gd,Y)Ba_2Cu_3O_{7-\delta}$ as the superconducting layer. As figure 1 shows, the final Cu-plate is not completely uniform. As manufactured, there are distinct, sharp interfaces between the REBCO, Ag and Cu layers. As will be shown later, these sharp interfaces were destroyed in the damaged zone produced during the spontaneous quenches.

The quench degradation was found on the inner coil 1, which consists of six double pancakes with a field constant of 36 mT A^{-1}. The bottom double pancake was deliberately wound with lower I_c tapes SP69, SP70 and SP72 (internal NHMFL designation) of about equal length, which did however still meet the 32 T conductor specification. It should be noted here that all three tapes were manufactured much earlier than those used in the final 32 T magnet at a time when properties were quite variable and generally lower. SP72, where damage occurred, is the middle tape that transitions from the top to the bottom pancake (figure 2). There are two solder joints inside the double pancake linking the three tape lengths with low resistances of less than 25 nΩ [23]. Figure 2(a) shows the prototype coil schematic, while figure 2(b) shows I_c versus field tilt in $\pm 18^\circ$ to the tape plane at 4.2 K for the three module six tapes (SP69, 70 and 72) using short samples cut from each tape end before they were wound into the coil. This was a standard measurement for the 32 T project because the field angle at the end pancakes of coil 2 is about 18°. This uncertainty to the *ab*-plane of REBCO occurs because the *ab* plane is offset from the tape plane by certain degrees and the tape plane itself is not perfectly flat. As a result, the critical currents with field tilt in $\pm 18^\circ$ are asymmetric. We generally use $B\|ab$ representing parallel field to the tape plane, and the designation of '+' or '−' 18° is arbitrary, depending on the positions of the tapes during measurements. Nonetheless, a key point here is that SP72 did have the lowest I_c and largest asymmetry. The angle between the *ab*-plane of REBCO and the tape plane is possibly the largest among the three. Therefore, the coil I_c was limited by tape SP72.

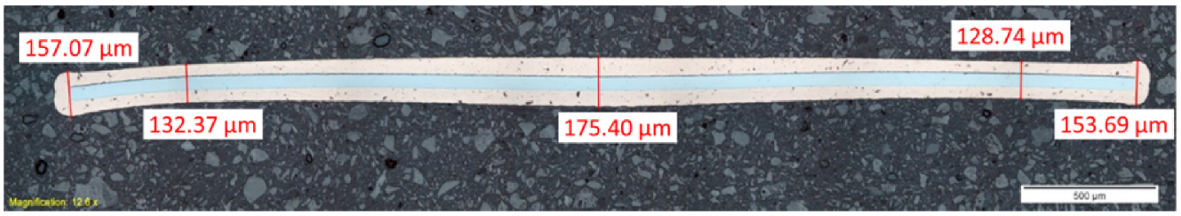

Figure 1. Cross-sectional view of one of the tapes used in the 32 T magnet made to the same specification as the presently studied tape SP72. The thickness across the width is not uniform.

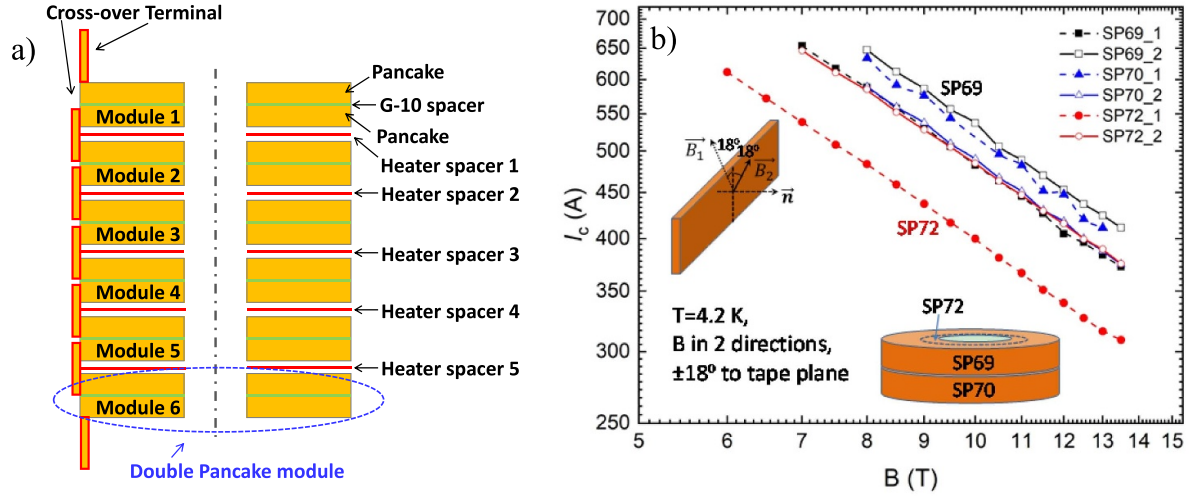

Figure 2. (a) Schematic of the prototype coil 1 [22]. (b) Transport I_c versus field tilt in $\pm 18^\circ$ to the tape plane at 4.2 K for the three module six tapes (SP69, 70 and 72) using short samples cut from each tape end before they were wound into the coil.

The accelerated fatigue testing was carried out in a background field of 14 T at a transport current ramp rate 44 times higher than the nominal 32 T ramp rate of 0.05 A s^{-1} (corresponding to a 1 h ramp from zero to full field in the 32 T magnet). Whereas the design HTS current value for the 32 T magnet at the time was 180 A, the peak current for fatigue cycling was 235 A. The first spontaneous quench occurred after 55 cycles at a peak field of 25 T and 229 A at a ramp rate of 2.2 A s^{-1} starting from 90 A. The second quench occurred at 220 A, with a ramp rate of 2.2 A s^{-1} starting from 200 A, while the third spontaneous quench occurred at 200 A even at the low ramp rate of 0.1 A s^{-1} from 0 A. All three quenches occurred in module 6 of coil 1. The spreading quench then activated the quench heaters in each case, but we note that these accelerated test conditions were outside the range for which the quench detection and protection system was designed to be effective. More specifically, the increase in the hysteresis loss caused larger temperature disturbance than normal operation, and the extremely localized voltage rise was averaged out before it could be detected whilst the current still increased rapidly. The heaters were fired too late to avoid damage.

After these quenches, coil 1 was disassembled, and signs of physical degradation were very obvious on the bottom double pancake, as shown in the image of the G10 spacer located in the middle of the double pancake (figure 3). Three burn marks (A, B, and C) can be clearly seen on the spacer, which was also permanently warped. The positions of the burn marks indicate that SP72 is the tape that initiated the spontaneous quenches.

2. Experimental details

The unwound tapes from the bottom double pancake were then measured at 77 K in YateStar [16, 17]. In order to have a quick estimation of the tape damage, remanent field Hall probe magnetization measurement without transport current was carried out first in order to avoid additional burn damage at any other weak spots in the tape. Separate in-field transport measurements were performed later after locating damaged zones, but regions with $I_c = 0$ were skipped to avoid further damage. The degraded regions located by the Hall scans were cut out for further study, especially by magneto-optical imaging (MOI) which can visualize the shape and size of the damaged areas [24]. Magnetization T_c traces were conducted in a magnetic property measurement system (MPMS SQUID magnetometer). To further assess the quenched regions, the Cu surface was etched away with APS-100 and $(NH_4)_2S_2O_8$ solutions and then examined in a Zeiss 1540 EsB scanning electron microscope (SEM) by energy-dispersive x-ray spectroscopy (EDS). Regions close to the damage zone were cut out for transmission electron microscopy (TEM) in a JEOL JEM-2011 microscope. To better understand the quench damage, an adjacent turn to the burned region of the quench center

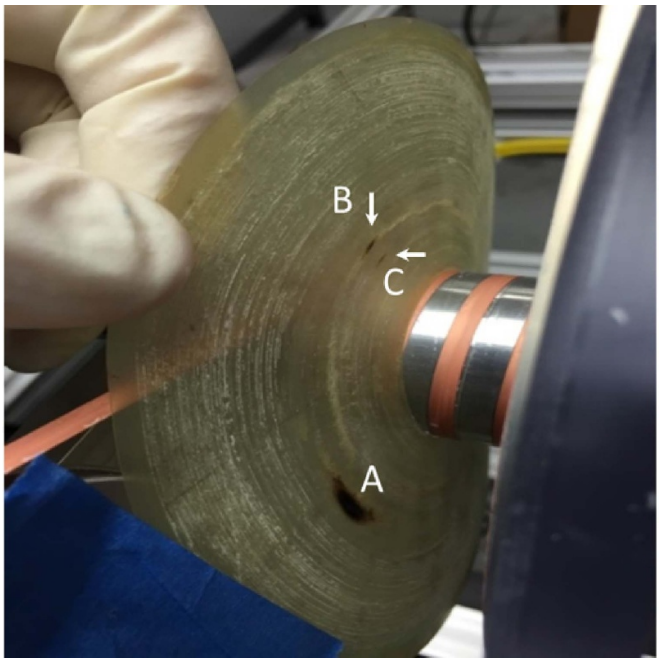

Figure 3. Picture of the G10 spacer in the middle of the damaged double pancake. The three zones are labeled A, B and C. The latter two are very localized and thus indicated by arrows. The spacer was permanently warped by the quenches.

was polished with a JEOL ion beam cross-section polisher and then examined by SEM and EDS.

3. Results

The position dependence of I_c at 77 K and 0.6 T of the three tapes from the damaged module is shown in figure 4(a). All three tapes have a much larger I_c for $B||c$ than for $B||ab$, indicating strong vortex pinning by dense, near optimal BZO nanorods [18], but it can be seen in figure 4(a) that there are significant lengthwise I_c fluctuations that we attribute to lengthwise variations of the vortex pinning center density and effectiveness [16]. The three damage zones *A*–*C* caused by the spontaneous quenches are all located in tape SP72, A being the most serious. YateStar transport measurements were not carried out for zone A in order to avoid further damage but the 2D magnetization map in figure 4(b) of zone A clearly show the impact of the burn damage on 25 neighboring turns. The map is obtained by measuring the remnant field of the tape with a seven-element Hall probe array [11, 25]. The inability to trap the field means losses of superconductivity. These Hall maps were then used to reconstruct the transport $I_c(x)$ at 77 K, 0.6 T shown in figure 4(c). Unlike the only partially damaged zones B and C, I_c of many turns in damage zone A drops to zero.

After the damaged sections were located, 10 mm long samples were cut out for the MO images shown in figure 5. The bright areas in the images represent damaged, non-superconducting regions incapable of generating screening currents that can inhibit flux entry. By comparing their sizes, we determined that turn 14 contains the center of zone A and

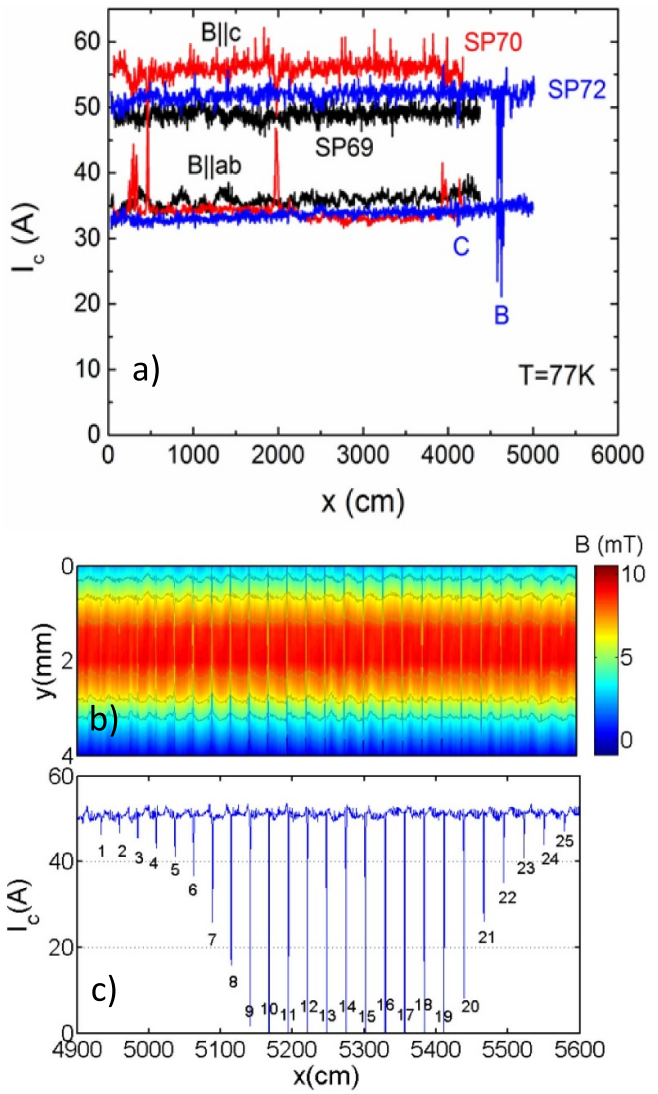

Figure 4. (a) Transport $I_c(x)$ measurement of the three tapes of the degraded double pancake ($T = 77$ K, $B = 0.6$ T). The damage zones were all found in SP72. Damaged zones B and C on SP72 are shown at left but no transport evaluation could be performed on the length containing zone A. (b) Two dimensional (2D) Hall magnetization map of 25 turns around damage zone A. (c) The reconstructed $I_c(x)$ according to (b) scaled to the measured transport data of undamaged regions with $B||c$, 0.6 T. The numbered damaged zones are all localized to regions located on a radial line through the central quench damage origin and are numbered from inner to outer. Turn 1 is the innermost turn with detectable degradation.

is very likely the place where the first of the three spontaneous quenches initiated. The damaged quench areas have almost perfectly circular shapes. However for samples away from the center, degradations start from both edges (e.g. sample A9). The small defect on the lower left edge of sample A13 is interesting but we are uncertain whether it was pre-existing and not related to the spontaneous quenches or perhaps a defect induced by the large thermal strains of the quench. For the less damaged zones B and C where I_c never dropped to zero, the damage was more localized and was better revealed by higher temperature MOI where J_c is lower and flux penetration easier.

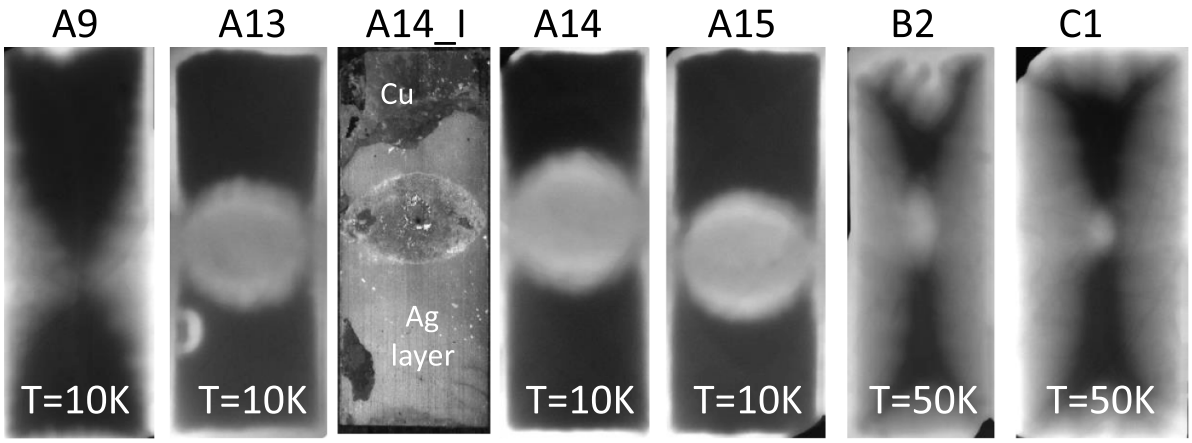

Figure 5. Magneto-optical (MO) images of samples (10 mm × 4 mm) cut out from the damage zones in turns 9, 13, 14 and 15 of zone A, turns 2 and 1 of zones B and C. A14_I is the surface optical image. Damage in zone A was imaged at 10 K and at 50 K for less heavily damaged samples from zones B and C. All images were made after zero field cooling (ZFC) and then applying fields of 120 mT for sample A9, B2 and C1, and 20 mT for A13–15. The bright regions indicate substantially complete flux penetration due to these regions not being superconducting. The dark regions are superconducting. The small defect at lower left on sample A13 might be pre-existing and not related to the quenches.

To better examine the most damaged sample A14, the Cu layer was etched away and examined by SEM. Figure 6(a) shows that there is an elliptically-shaped dark region with a sharp interface to the neighboring Ag, rather than the circular shape of the MO images (figure 5). The black spot is about 2.6 mm along the conductor axis and about 3.5 mm transverse, both dimensions being smaller than those observed MO in figure 5. As we discuss later, we believe that the sharp interface marks the boundary between smooth Ag that remained solid and the rougher, blackened area where the Ag melted and mixed with the Cu overlayer to make a low melting (at least 779 °C is required) eutectic alloy. Outside the black spot, as in figure 6(b), we believe that the temperature was lower but there was still damage to the REBCO, as indicated by the larger MO damage zones illustrated in figure 5. The SEM image shows that the Ag surface is bumpy at the edge of the black spot, especially for the parts close to the tape edges. Inside the dark spot many craters can be seen without either Ag or REBCO.

Figure 6(b) shows a transverse cross-sectional view (focused ion beam (FIB)) of the region just to the left edge of the blackened Ag spot made along the line indicated by the dashed line marked in figure 6(a). Here the Ag-REBCO interface remains sharp but the REBCO layer itself has separated into two layers, the top without obvious damage but the bottom blown apart by the heat of the quench and with much porosity. Figure 6(c) shows that the REBCO thickness, though highly expanded in the quench zone, falls back to its unperturbed value 150–200 μm away from the burn zone boundary.

The extreme localization of damage in the burn zone is also reflected in SQUID magnetization T_c traces. Figure 7 compares warming T_c transitions in 1 mT after ZFC to 40 K of the burn zone of sample A14, its immediate neighbors and a control sample far away from it. The middle burn-zone piece is about 4 mm × 4 mm and thus contains regions outside the burn zone that do prevent flux penetration. Indeed all four samples show superconducting transitions. Although T_c of the heavily damaged middle piece is about 3 K lower than others, it is progressive over a range of about 50 K, suggesting maintenance of the REBCO structure with some expulsion of O and loss of T_c due to warming by the burn zone. By contrast the neighboring top and bottom pieces have very similar transitions to that of the control sample. These T_c transitions also speak to the intense localization of the damage in the burn zone and the negligible longitudinal quench propagation velocity.

During the Cu-etching of sample A14, it was found that the 50 μm thick Cu surface layer showed no obvious top surface damage but became porous close to the REBCO in the center of the burn zone. To explore this observation further, the damaged region of neighboring turn A15 was cut in half, its cross-section ion-beam polished and then imaged as in figure 8(a). In contrast to the still distinct Cu, Ag and REBCO interfaces of the sample taken from outside the burn zone in figure 6, here, inside the burn zone of turn A15, the boundaries between the Cu, Ag and REBCO layers have almost totally disappeared. EDS analyses at positions A–E have EDS spectra in figure 8(b) that confirm that a Cu–Ag alloy is present in all regions A–E, even in regions A–C which was the location of the original pure REBCO layer. Although the buffer layer and substrate interfaces remain well defined, there is no longer any clear demarcation between REBCO, Ag and Cu layers. Figure 8(c) shows the EDS of the mixed-melt lump marked in figure 8(a), for which the (Y,Gd):Ba:Cu ratio largely deviates from the expected 1:2:3 atom ratio, suggesting REBCO melting during the quench. Even more directly suggestive of melting are the analyses of Ag and Cu. Table 1 shows that all five regions examined have Ag present in amounts ranging from 6 wt% to 68 wt%. Given the quite distinct separation of the REBCO, Ag and Cu layers in the manufactured conductor (figure 1), the mixing attested to by table 1 is evidence that the

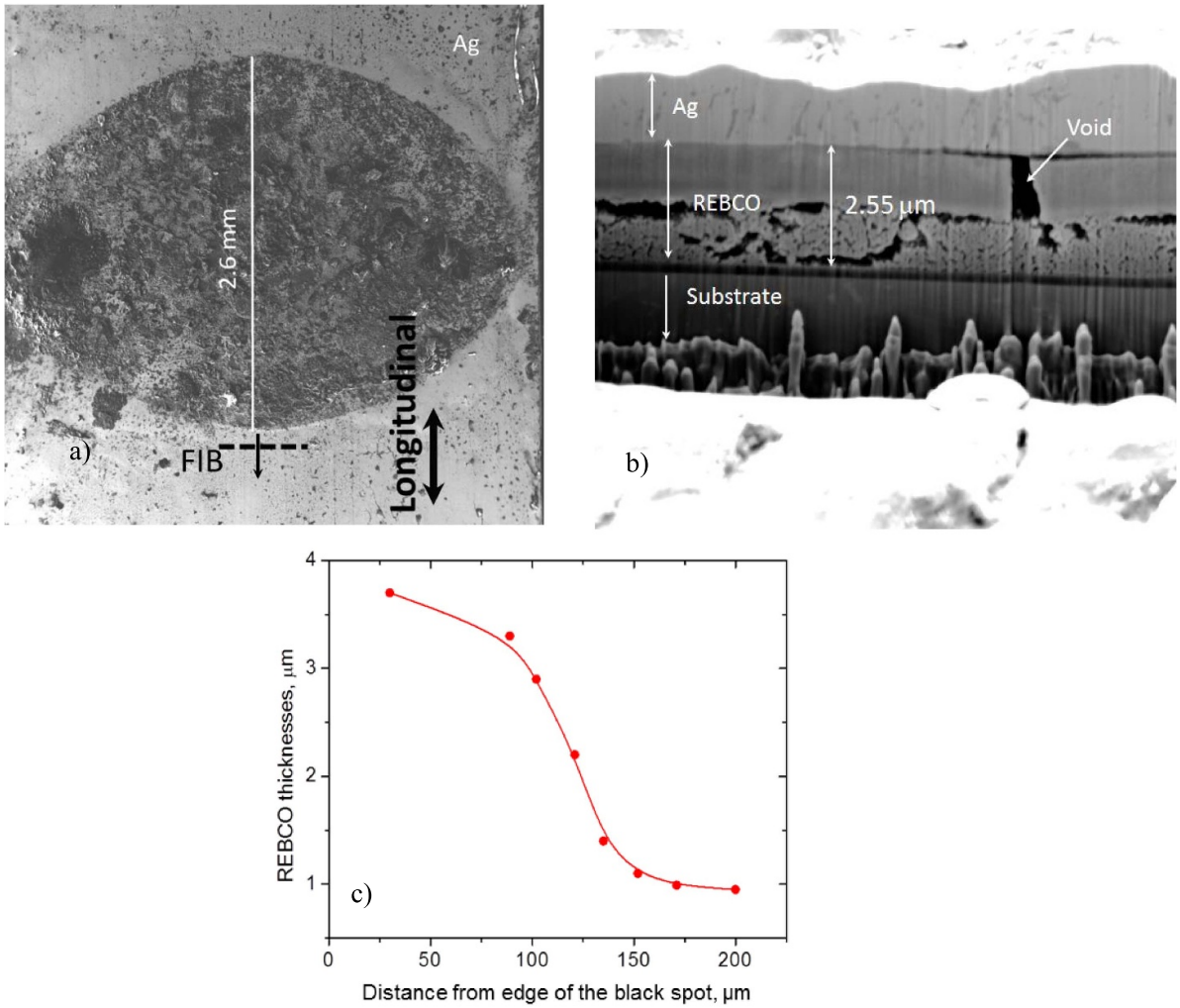

Figure 6. (a) SEM top view of the elliptical black spot observed after etching away the Cu layer. The spot is 2.6 mm wide along the tape axis and about 3.3 mm wide across the tape. (b) SEM transverse cross-sectional view of a FIB section indicated by the dashed line in image (a). (c) REBCO thickness vs distance from the edge of the black spot on the Ag. The measured locations are along the solid black arrow crossing the dashed line where the FIB cross-section was made.

temperature reached at least 779 °C, the melting temperature of the eutectic composition of Cu71.9%Ag. That the highest Ag content is a little lower suggests that even higher temperatures were reached, as also does the highly porous structure of the REBCO layer in the burn zone and the off-stoichiometric EDS data in figure 8(c).

Because we now know that the 4 K high field properties of the tapes are closely tied to the perfection of the BZO nanostructures [19], we then compared the nanostructure by TEM of samples immediately located next to the burn zone with samples cut close to but apart from the burn zone under the assumption that the cause of the local burn out might have been variations in the $BaZrO_3$ and RE_2O_3 nanostructure. Accordingly we cut out a sample from turn A18 from a region about 1 mm away from the edge of the damage zone (recall that this is not a primary damaged zone but one secondarily damaged by the intense heating in turn 14). Figure 9 shows that the BZO nanorod diameters are closely clustered in the range of 5.5–7.5 nm, mostly around 6 nm, which is the expected optimum range for highest J_c in these tapes [18, 19]. No BZO nanoparticles or large precipitates were observed. Thus the nanostructure at this point appears to be what manufacturing desired. The planar defects indicated by the white arrows are the consequences of the quench heat and have caused 30% increase of the thickness of REBCO.

By contrast study of the regions where the spontaneous quenches initiated showed a different story. Samples were cut 3 to 4 mm away from the black spot edges of the centers of turn A14, B2 and C1. Figure 10 shows the cross-sectional view of these samples. In the zone A sample very close to the burn-initiation zone, many BZO nanorods have a large diameter of order 10–16 nm and are only 40–50 nm long. RE_2O_3 precipitates as indicated by the arrows lying in the *ab*-plane are also obvious, which usually favors the vortex pinning in the *ab*-direction at lifted temperature [17]. As discussed later, we expect this nanostructure to be far from optimum and to set up local low J_c conditions. In the less critically damaged zone B, the average length of BZO nanorods is a little longer than that

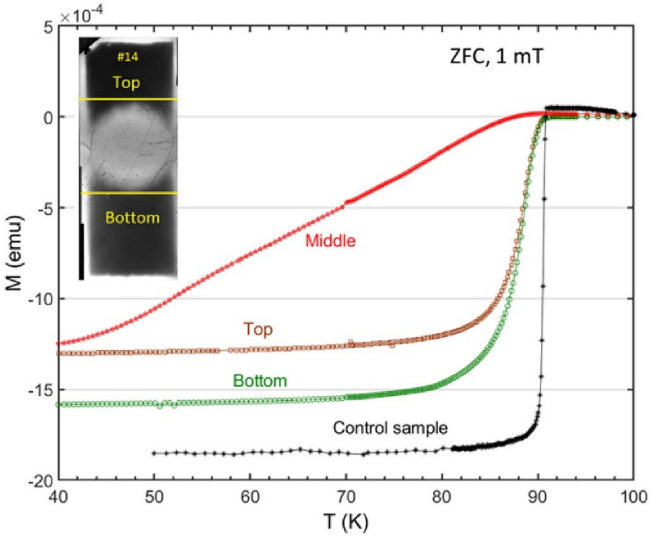

Figure 7. Temperature dependence of magnetization after ZFC to 40 K, then applying H = 1 mT during warming for the three pieces of sample A14 (Cu has been etched away) and a control sample taken far away from the damage zone.

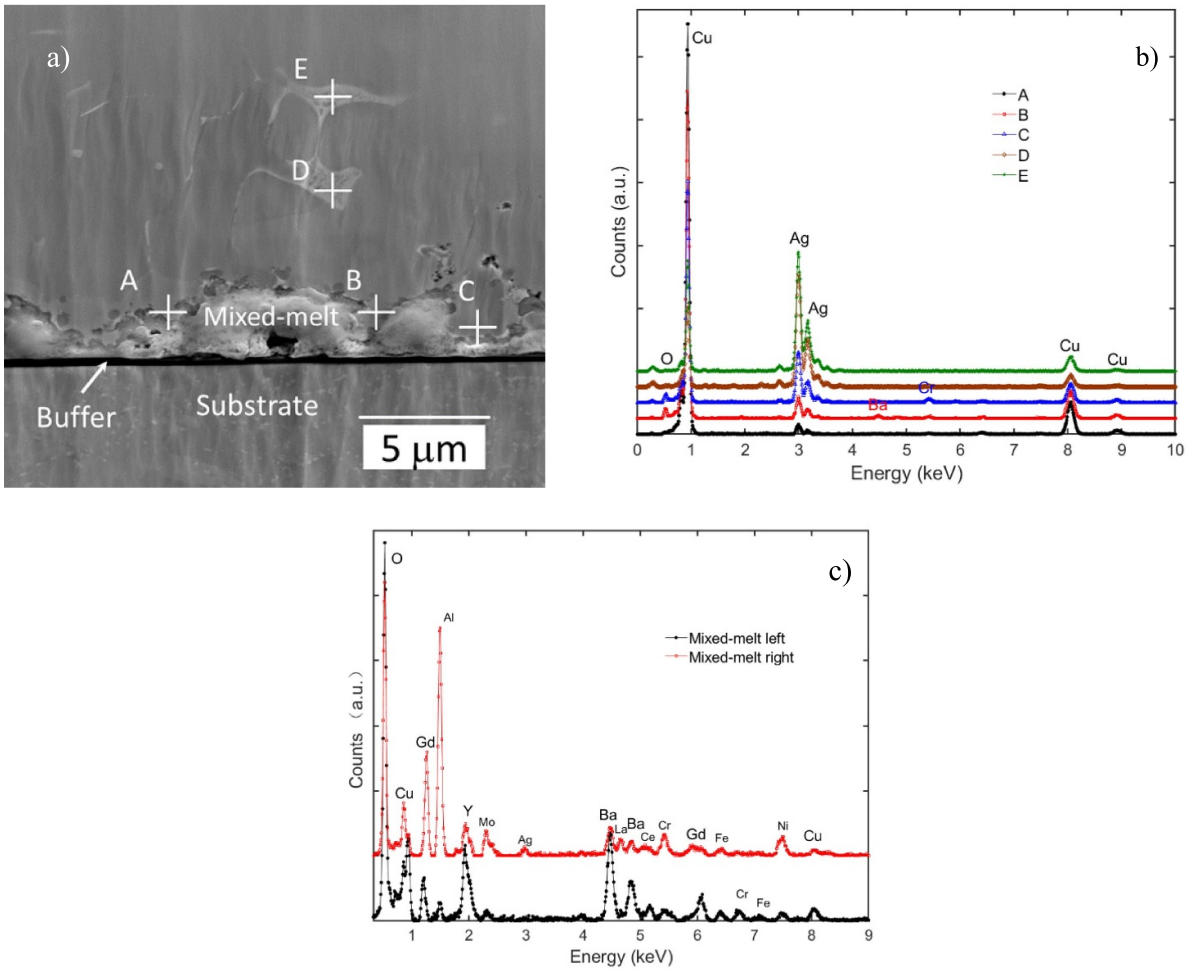

Figure 8. (a) Ion-beam polished SEM cross-section of sample A15. A–E are positions where EDS analyses were performed. (b) EDS spectra of A–E. (c) EDS of the mixed-melt lump marked in (a), on which two spots were examined. Besides Cu and Ag, there are also other elements either from the buffer layer or the Hastelloy substrate. The REBCO spectra vary but clearly all deviate from that of stoichiometric RE123.

Table 1. Weight percentage of Ag in Cu–Ag alloy at positions indicated in figure 8.

Location	A	B	C	D	E
Wt% of Ag	6.02	13.90 (with 2.26% O)	35.4 (with 2.61% O)	62.83	68.20

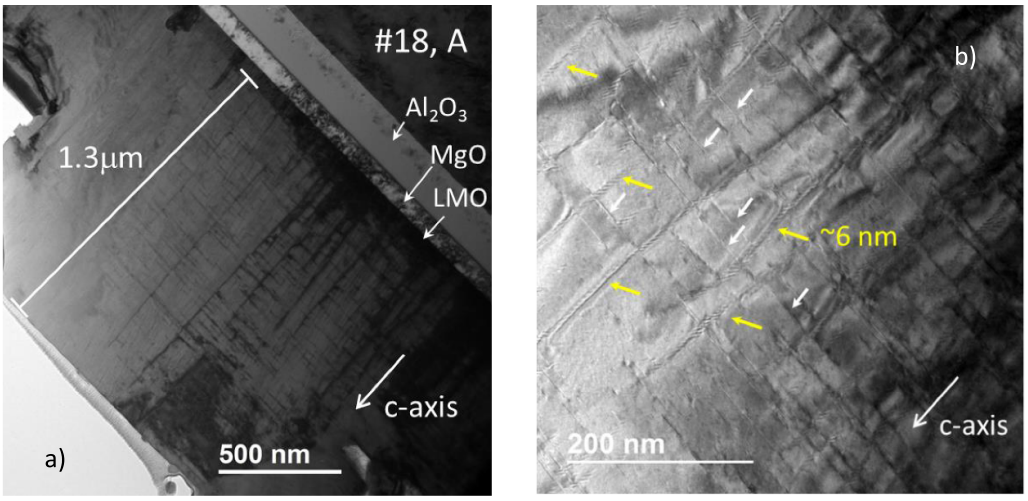

Figure 9. TEM cross-sectional view of a region on turn A18. (a) A large-area, low-magification view. The buffer layers, Al_2O_3, MgO and $LaMnO_3$ (LMO) are indicated by arrows. (b) A higher-magnification view. BZO nanorods indicated by yellow arrows have diameters of about 6 nm. The planar defects indicated by white arrows are about 1 to 2 nm thick.

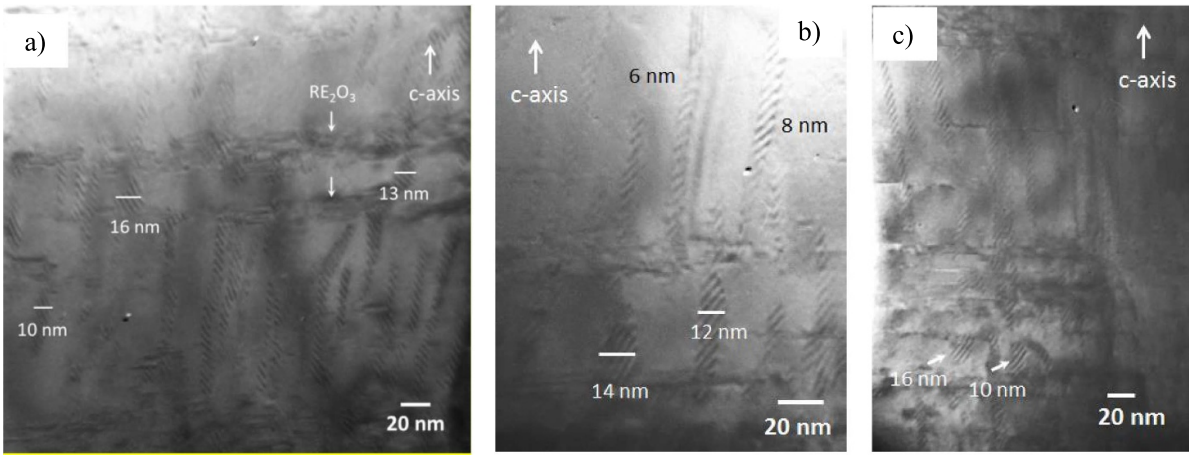

Figure 10. (a), (b) and (c) TEM cross-sectional view of samples from turn A14, B2 and C1, respectively. Samples were cut 3 to 4 mm away azimuthally from the burned zone centers. The BZO morphology is very different from the control, undisturbed area imaged in figure 9. Many much larger and shorter BZO nanorods and nanoparticles with diameter over 10 nm are present.

in zone A, but thick BZO nanorods with diameter larger than 10 nm are present as in zone A. The BZO nanorod diameter is most uniform in the zone C sample. Thus there is a clear difference between the BZO morphology of primary damaged zones A, B and C and neighboring undamaged zones. A recent study of the wide variety of properties observed in the more than 100 lengths of REBCO used for the 32 T magnet shows that fluctuations in the density, spacing and morphology of the BZO play an enormous role in determining the magnitude and field dependence of J_c [19], thus implicating the local fluctuations of nanostructure in the damage observed in our study.

4. Discussion

The key finding of our study of the quench damage to this 32 T prototype coil is that damage occurred in three highly localized regions of the lowest I_c tape located in one end pancake where the operating current I_{op} had the smallest I_c margin. The damage was intensely localized to regions smaller than 4 mm in diameter, while regions less than a tape width away remaining superconducting, even though there is microstructural evidence of local melting of REBCO, Ag and Cu that could only occur with a local temperatures that achieved between 800 °C

and 1000 °C. We set up our discussion around the following key points:

(a) the damage behavior observed was not at all according to our expectations of propagating fatigue cracks emanating, for example, from slit edge cracks of the type seen in our recent post mortem of the 40–45 T no insulation (NI) Little Big Coils [11, 25].
(b) In contrast it appears that the damage is a direct consequence of two effects:
    1. rapid ramping at 44 times faster rate than the previous normal (i.e. the planned 32 T ramp rate of 0.5 T min^{-1}) so as to be able to achieve a reasonable number of fatigue cycles in a day. Apparently, the fast ramp generated sufficient heating of the bottom double pancake to drive the transport current I_{op} close to local I_c, well above the planned operating point of 32 T service.
    2. Based on YateStar scans of other tapes [16, 17] made to the same specification as the present tapes (there actually was no 4 K specification for the tapes, only a 77 K, self-field I_c specification) and the BZO nanostructural morphology analysis shown in figures 9 and 10, it appears very plausible that there were highly localized regions of low I_c present that only activated as damage zones during the fast fatigue ramping campaign which caused the I_{op}/I_c ratio to locally exceed 1 and then to instigate burn damage in the three specific zones A, B and C.

In this coil, current sharing between turns is not possible because each REBCO turn is separated from the next by a co-wind of stainless steel insulated with a sol–gel SiO_2 coating. Thus any fluctuation of critical current density in the tape which brings I_{op} close to I_c must cause the excess current $I_{op} > I_c$ to be locally passed into the Cu where it generates heat. Since the I_{op}/I_c ratio under standard slow ramp conditions was reasonably below I_c, it seems likely that the coil entered danger only during the last, fast-ramp campaign. To be specific, the previous slow charging had brought I_{op} up to 264 A in 15 T background without any quenches [22]. It seems plausible to reconstruct the damage as starting from highly localized low I_c zones A–C, which started to shed current into the copper, well below the peak 235 A I_{op} of the fatigue tests. The ramp rate pattern was changed slightly between cycle 55 and 56. We postulate that thermal equilibrium barely existed during the first 55 fatigue cycles and AC-losses in the 56th cycle were slightly higher, causing the first spontaneous quench and started the process of irreparable pancake damage presented here.

As part of the quench protection plan of the magnet a thermal model of the winding was constructed in order to understand temperature rise during quench. To assess this damage, the assumption of a 1 mm wide transverse defect in the REBCO layer formed by sudden fatigue crack growth at $I = 200$ A, $B = 15$ T was explored, the excess current bypassing through the Cu matrix. The temperature dependent anisotropic thermal diffusivity of the winding was included in the simulation as is detailed in [26–28]. Figure 11 shows the time dependence of temperature at the defect. It demonstrates that the Cu–Ag eutectic temperature of 779 °C can be reached very rapidly, in fact within 1.5 s. But, because of the intense localization of the defect, both in the model and in reality, the peak voltage remains below 0.5 mV, which makes its detection very difficult. In fact the quench only triggered the protection system after it was too late to prevent the localized burning.

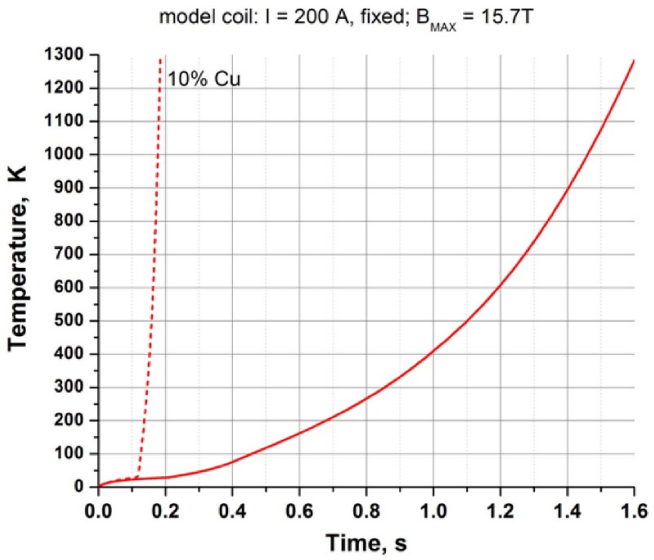

Figure 11. Simulation of a localized unprotected quench initiated in the region with a 1 mm × 4 mm transverse defect. The temperature dependent anisotropic thermal diffusivity was included appropriately. The solid line is the case with 100 μm thick Cu (nominal) in the REBCO tape, and the dashed line is with 10 μm thick Cu (artificially reduced in calculation to assess the effect of the amount of copper on the rate of temperature rise).

The plausibility of the peak temperature simulation receives experimental confirmation from the MO, SEM and TEM images, EDS analyzes, and SQUID T_c traces in figures 5–10. Figures 5 and 6 confirm the intense localization of the damage considered in the model while figure 8 confirms that the burn zone was intense enough to generate REBCO–Ag–Cu alloy. The high percentage of Cu close to the original REBCO layer indicates that the actual temperature was higher than the 779 °C eutectic temperature of Cu and Ag. Our estimation for the peak temperature is then between 900 °C and 1000 °C.

We believe that important clues to the root cause of the quench lie in the microstructure, especially in the significant variability of the BZO nanorod morphology shown in figures 9 and 10. We know that the more than 130 tape lengths used for the real 32 T magnet exhibited a considerable spread of properties, as judged from tape end I_c tests performed as part of the quality control. We also know that REBCO coated conductors of the vintage used for this test coil often showed I_c (77 K, 0.6 T) fluctuations and occasional local inversion of the anisotropy of I_c for B parallel and perpendicular to the tape plane in fields of 0.6–1 T [17] that we attribute to nanostructure fluctuations, above all to BZO nanorod size and density

variations. This conclusion is now well established by the recent, detailed study of Francis *et al* [19]. With all of this as background we believe that the electron microscope images of figures 8–10 provide a consistent story with which to understand the quench damage that occurred in this coil.

Turning to more specifics, we cite the recent detailed studies of the wide range of properties exhibited within the 132 tape lengths (all made to the same advanced pinning formula) used for the 32 T magnet, where Francis *et al* showed that the general expression for $J_c(B, T)$ heavily depends very markedly on the BZO nanostructure [19]

$$J_c(B,T) = J_c^* B^{-\alpha} \exp\left(\frac{-T}{T_0(B)}\right).$$

where J_c^*, α and T_0 are parameters obtained by fitting the experimental data. The key point of this methodology is to disentangle the strong pinning generated by BZO and RE_2O_3 that is operative at all temperatures up to T_c from additional oxygen defect point pinning whose concentration is determined by the size, density and especially the BZO nanorod spacing. Comparison of the nanostructure of SP72 away from the quench origin (figure 9) shows well-formed BZO nanorods and a rather uniform, dense REBCO layer. The thickness of the good region is about 0.95 μm as shown in figure 6(c). A separate measurement with perpendicular field gives an I_c(14 T, $B\|c$, 4.2 K) $\approx$ 195 A, correspondingly J_c(14 T, $B\|c$, 4.2 K) $\approx$ 5.13 MA cm^{-2}. The data presented by Francis for SP139 (J_c(14 T, $B\|c$, 4.2 K) = 5.18 MA cm^{-2} with BZO nanorod diameter $\sim$8 nm with a 3.4 vol% BZO) [19] appears close to the behavior of SP72 with $\sim$6 nm diameter BZO nanorods. Evidently, the perturbation to the non-optimum BZO seen in figure 10(a) degrades the J_c, setting up the conditions for localized burnout seen in figure 5.

We finally note the essential difference between the failure seen here and that in our >40 T Little Big Coils made without insulation working at much higher conductor current densities and stresses [11], where cracks were accompanied by evident plastic deformation of the tape which occurred before quench. Such issues did not appear for this prototype coil even after fatigue testing. For the reasons described , we propose that localized vortex pinning anomalies initiate these spontaneous quenches. The accelerated ramping of the current generated sufficient heating of the bottom module to drive the transport current I_{op} close to the tape's average I_c. The uniformity of the nanostructure under such circumstances thus becomes crucial. A proper lengthwise characterization of the vortex pinning variations may thus be essential for the avoidance of unexpected quenches when high I_{op}/I_c ratios are planned. In particular, concerns are mounting with respect to screening current stress enhancements, for which using tapes with deliberately lowered I_c is a possible countermeasure [29]. Unfortunately the standard remnant field Hall Probe scanning device TapeStar employed by virtually all coated conductor manufacturers is much more sensitive to interruptions of I_c due to scratching or other blocking defects than to vortex pinning variations.

5. Summary and conclusions

We deconstructed the innermost coil of the 32 T prototype magnet that suffered damage in a final fatigue testing campaign after being deliberately quenched many times in a 14 or 15 T background field. We found three damaged zones in the bottom double pancake with very small sizes (4 mm diameter at most) that clearly indicate steady state heating with almost zero normal zone propagation velocity. The appearance of Cu–Ag alloy after the spontaneous quenches indicates that the peak temperature exceeded the 779 °C Cu–Ag eutectic melting temperature. Short BZO nanorods ($\sim$40 nm), nanoparticles (10–16 nm) and RE_2O_3 precipitates observed 3 and 4 mm away from the melt zone centers are likely pre-existing and indicate locally perturbed (and degraded) vortex pinning capability. We believe that the spontaneous quenches were initiated when a hysteresis-loss induced temperature increase produced small local regions with steady state Cu stabilizer dissipation that were below the voltage detection threshold of the quench protection system. We believe that these defects, rather than the expected fatigue-induced cracks for which no evidence appeared in our YateStar scans, were what triggered the damage to this coil.

Data availability statement

The data generated and/or analyzed during the current study are not publicly available for legal/ethical reasons but are available from the corresponding author on reasonable request.

Acknowledgments

We would like to thank Dr. Yifeng Su for his help on TEM. This work was performed at the National High Magnetic Field Laboratory in Tallahassee FL which is supported by the National Science Foundation under Cooperative Agreement DMR-1644779 and by the State of Florida.

ORCID iDs

X Hu https://orcid.org/0000-0002-6553-3647
A A Polyanskii https://orcid.org/0000-0002-5977-5324
F Kametani https://orcid.org/0000-0002-1067-9331
J Jaroszynski https://orcid.org/0000-0003-3814-8468
D C Larbalestier https://orcid.org/0000-0001-7098-7208

References

[1] Hazelton D W, Selvamanickam V, Duval J M, Larbalestier D C, Markiewicz W D, Weijers H W and Holtz R L 2009 Recent developments in 2G HTS coil technology *IEEE Trans. Appl. Supercond.* **19** 2218–22
[2] Markiewicz W D, Weijers H W, Noyes P D, Trociewitz U P, Pickard K W, Sheppard W R, Jaroszynski J J, Xu A, Larbalestier D C and Hazelton D W 2010 33.8 tesla with a

$YBa_2Cu_3O_{7-x}$ superconducting test coil *AIP Conf. Proc. Trans. OF THE CRYOGENIC ENGINEERING Conf.—CEC: Advances in CRYOGENIC ENGINEERING* vol 1218 (AIP Publishing) pp 225–30

[3] Trociewitz U P, Dalban-Canassy M, Hannion M, Hilton D K, Jaroszynski J, Noyes P, Viouchkov Y, Weijers H W and Larbalestier D C 2011 35.4 T field generated using a layer-wound superconducting coil made of (RE)$Ba_2Cu_3O_{7-x}$ (RE = rare earth) coated conductor *Appl. Phys. Lett.* **99** 202506

[4] Zhang M, Yuan W, Hilton D K, Canassy M D and Trociewitz U P 2014 Study of second-generation high-temperature superconducting magnets: the self-field screening effect *Supercond. Sci. Technol.* **27** 095010

[5] Yoon S, Kim J, Cheon K, Lee H, Hahn S and Moon S-H 2016 26 T 35 mm all-$GdBa_2$ Cu_3O_{7-x} multi-width no-insulation superconducting magnet *Supercond. Sci. Technol.* **29** 04LT04

[6] Awaji S, Watanabe K, Oguro H, Miyazaki H, Hanai S, Tosaka T and Ioka S 2017 First performance test of a 25 T cryogen-free superconducting magnet *Supercond. Sci. Technol.* **30** 065001

[7] Li Y, Park D, Yan Y, Choi Y, Lee J, Michael P C, Chen S, Qu T, Bascuñán J and Iwasa Y 2019 Magnetization and screening current in an 800 MHz (18.8 T) REBCO nuclear magnetic resonance insert magnet: experimental results and numerical analysis *Supercond. Sci. Technol.* **32** 105007

[8] Liu J *et al* 2020 World record 32.35 tesla direct-current magnetic field generated with an all-superconducting magnet *Supercond. Sci. Technol.* **33** 03LT01

[9] Suetomi Y *et al* 2021 Quench and self-protecting behaviour of an intra-layer no-insulation (LNI) REBCO coil at 31.4 T *Supercond. Sci. Technol.* **34** 064003

[10] Hahn S 2016 Superconducting insert magnet generates new record field of 40.2 teslas (available at: https://nationalmaglab.org/magnet-development/applied-superconductivity-center/publications-asc/highlights-asc/40-2-tesla-superconducting-insert-magnet)

[11] Hahn S *et al* 2019 45.5-tesla direct-current magnetic field generated with a high-temperature superconducting magnet *Nature* **570** 496–9

[12] Selvamanickam V *et al* 2007 Recent progress in second-generation HTS conductor scale-up at superpower *IEEE Trans. Appl. Supercond.* **17** 3231–4

[13] Zhang Y, Lehner T F, Fukushima T, Sakamoto H and Hazelton D W 2014 Progress in production and performance of second generation (2G) HTS wire for practical applications *IEEE Trans. Appl. Supercond.* **24** 1–5

[14] Sundaram A *et al* 2016 2G HTS wires made on 30 μm thick Hastelloy substrate *Supercond. Sci. Technol.* **29** 104007

[15] Majkic G, Pratap R, Paidpilli M, Galstyan E, Kochat M, Goel C, Kar S, Jaroszynski J, Abraimov D and Selvamanickam V 2020 In-field critical current performance of 4.0 μm thick film REBCO conductor with Hf addition at 4.2 K and fields up to 31.2 T *Supercond. Sci. Technol.* **33** 07LT03

[16] Hu X, Rossi L, Stangl A, Sinclair J W, Kametani F, Abraimov D, Polyanskii A, Coulter J Y, Jaroszynski J and Larbalestier D C 2017 An experimental and analytical study of periodic and aperiodic fluctuations in the critical current of long coated conductors *IEEE Trans. Appl. Supercond.* **27** 1–5

[17] Rossi L, Hu X, Kametani F, Abraimov D, Polyanskii A, Jaroszynski J and Larbalestier D C 2016 Sample and length-dependent variability of 77 and 4.2 K properties in nominally identical RE123 coated conductors *Supercond. Sci. Technol.* **29** 054006

[18] Xu A, Braccini V, Jaroszynski J, Xin Y and Larbalestier D C 2012 Role of weak uncorrelated pinning introduced by $BaZrO_3$ nanorods at low-temperature in (Y,Gd)$Ba_2Cu_3O_x$ thin films *Phys. Rev.* B **86** 115416

[19] Francis A, Abraimov D, Viouchkov Y, Su Y, Kametani F and Larbalestier D C 2020 Development of general expressions for the temperature and magnetic field dependence of the critical current density in coated conductors with variable properties *Supercond. Sci. Technol.* **33** 044011

[20] Weijers H W *et al* 2010 High field magnets with HTS conductors *IEEE Trans. Appl. Supercond.* **20** 576–82

[21] Markiewicz W D *et al* 2012 Design of a superconducting 32 T magnet with REBCO high field coils *IEEE Trans. Appl. Supercond.* **22** 4300704

[22] Weijers H W *et al* 2014 Progress in the development of a superconducting 32 T magnet with REBCO high field coils *IEEE Trans. Appl. Supercond.* **24** 1–5

[23] Weijers H W *et al* 2016 Progress in the development and construction of a 32-T superconducting magnet *IEEE Trans. Appl. Supercond.* **26** 1–7

[24] Polyanskii A A, Cai X Y, Feldmann D M and Larbalestier D C 1999 Visualization of magnetic flux in magnetic materials and high temperature superconductors using the Faraday effect in ferrimagnetic garnet films *Nano-Crystalline and Thin Film Magnetic Oxides NATO Science Series* ed I Nedkov and M Ausloos (Dordrecht: Springer Netherlands) pp 353–70

[25] Hu X *et al* 2020 Analyses of the plastic deformation of coated conductors deconstructed from ultra-high field test coils *Supercond. Sci. Technol.* **33** 095012

[26] Gavrilin A V *et al* Comprehensive quench analysis of the NHMFL 32 T all-superconducting magnet system *CHATS on Applied Superconductivity* (Bologna: University of Bologna) *(14–16 September 2015)* (available at: https://indico.cern.ch/event/372812/contribu-tions/1792178/attachments/1158596/1667005/19_Gavrilin.pdf

[27] Gavrilin A V and Weijers H W Comprehensive modelling study of quench behaviour of the NHMFL 32 T all-superconducting magnet system. Input data and methodology aspects *5th Int. Workshop on Numerical Modelling of High Temperature Superconductors ("HTS Modelling 2016")* (*Bologna, Italy*, *15–17 June 2016*) (available at: www.die.ing.unibo.it/pers/morandi/didattica/Temporary-HTS-Modelling2016/Gavrilin.pdf)

[28] Hilton D K, Gavrilin A V and Trociewitz U P 2015 Practical fit functions for transport critical current versus field magnitude and angle data from (RE)BCO coated conductors at fixed low temperatures and in high magnetic fields *Supercond. Sci. Technol.* **28** 074002

[29] Kolb-Bond D J, Berrospe-Juarez E, Bird M, Dixon I R, Weijers H W, Trillaud F, Zermeno V M R and Grilli F 2020 Computing strains due to screening currents in REBCO magnets *IEEE Trans. Appl. Supercond.* **30** 1–5